Fermi surface of novel borides: MgB_2 and CaB_6

2007 J. Phys.: Condens. Matter 19 355003

(http://iopscience.iop.org/0953-8984/19/35/355003)

IOP PUBLISHING JOURNAL OF PHYSICS: CONDENSED MATTER

J. Phys.: Condens. Matter **19** (2007) 355003 (17pp) doi:10.1088/0953-8984/19/35/355003

Fermi surface of novel borides: MgB_2 and CaB_6

S Souma and T Takahashi

Department of Physics, Tohoku University, Sendai 980-8578, Japan

E-mail: t.takahashi@arpes.phys.tohoku.ac.jp

Received 29 September 2006
Published 20 August 2007
Online at stacks.iop.org/JPhysCM/19/355003

Abstract

We have performed systematic high-resolution angle-resolved photoemission spectroscopy (ARPES) on two novel boride compounds, MgB_2 and CaB_6, to study the electronic structure near the Fermi level relevant to the anomalous physical properties (superconductivity and ferromagnetism) observed in these compounds. In MgB_2, we have succeeded in separately observing two superconducting gaps which originate in the σ and π bands, respectively, and thereby established the two-band superconductivity. ARPES measurements on AlB_2, which is a non-superconducting isostructural reference compound of MgB_2 with an additional electron in a unit cell, indicates the importance of the σ band for the superconductivity. In CaB_6, we observed an energy gap of 1 eV at the X point in the Brillouin zone, which suggests that CaB_6 is intrinsically a large-gap semiconductor. This observation requires reconsideration of the excitonic-insulator model to explain the anomalous ferromagnetism in CaB_6.

1. Introduction

The Fermi surface, defined as a locus of gapless excitation of electrons in momentum space, characterizes essential physical properties of metals. Recent remarkable progress of both energy and momentum resolutions in angle-resolved photoemission spectroscopy (ARPES) enables us to experimentally determine the Fermi surface with considerable accuracy. One of the distinguished merits of ARPES is its unique capability to select a particular point in the Brillouin zone and observe the local electronic structure in the momentum space. This becomes a great advantage when we study materials which have complicated Fermi-surface sheets relevant to the anomalous physical properties.

Recently, two intriguing discoveries in borides have stimulated extensive research activities. One is the 'high-temperature' superconductivity ($T_c \sim 39$ K) observed in MgB_2 [1] and another is the anomalous high-temperature weak ferromagnetism ($T_C \sim 600$ K) in La-doped CaB_6 [2]. The mechanism of superconductivity in MgB_2 has been intensively studied and several theoretical models have been proposed [3–9]. Among them, the most discussed is the two-band model [3, 4], where electrons in the σ band strongly couple with

phonons confined within the honeycombed boron layer while electrons in the π band have a weaker coupling. Based on the strong anisotropy of electron–phonon coupling between σ and π bands, this model predicts a large superconducting gap on the σ Fermi surface and a small or negligible gap on the π Fermi surface. Several experiments such as the specific-heat measurements [10, 11], Raman [12, 13], tunnelling [14–18] and photoemission [19] spectroscopies propose the existence of two different superconducting gaps, supporting the two-band model. However, the lack of momentum-resolved information in these experiments makes it difficult to exclude other possibilities for two superconducting gaps in MgB_2.

The observed peculiar weak ferromagnetism at relatively high temperatures in CaB_6 has been a target of intensive theoretical studies. So far, two different models, the excitonic-insulator model [20–23] and the low-density electron–gas model [24, 25], have been proposed. The excitonic-insulator model assumes the semi-metallic band structure with a small overlapping between the valence and conduction bands at the X point in the Brillouin zone. The model predicts that the formation of excitons due to the interaction of the hole and electron bands produces a small energy gap at the X point, and the subsequent electron doping by replacing Ca with La atoms leads to the ferromagnetism because of the imbalance between the up- and down-spin electrons [20–23]. In contrast, the low-density electron–gas model does not assume the semi-metallic nature of the parent compound (CaB_6), explaining that the ferromagnetism emerges in a certain small region of the electron density. Although a key to distinguish these two models is to directly see the electronic structure and Fermi surface around the X point, no momentum-resolved measurements have been performed to date.

In order to solve these problems described above, we have performed ARPES on MgB_2, CaB_6, and related compounds. In MgB_2, we observed that a superconducting gap opens both on the σ and π Fermi surfaces and, more importantly, the size of superconducting gap is much larger in the σ band than in the π band. We have also performed ARPES measurements on AlB_2, a non-superconducting isostructural reference compound of MgB_2, to elucidate the role and importance of the σ band for superconductivity. In CaB_6, on the other hand, we have performed careful ARPES measurements around the X point with both ultraviolet (UV) light and x-rays, and found that CaB_6 is intrinsically a semiconductor with a 1 eV gap at the X point, contrary to the assumption of the excitonic-insulator model.

2. Experiments

Single crystals of MgB_2 were grown in a closed stainless steel tube filled with argon gas, while those of AlB_2 were grown by the Al-flux method [26]. The typical size of MgB_2 crystals for ARPES measurements is $100 \times 100 \times 10$ μm^3. CaB_6 and $Ca_{0.995}La_{0.005}B_6$ single crystals were grown by the floating zone (FZ) method and the Al-flux method, respectively. We have confirmed the weak ferromagnetism and metallic conductivity of samples used for ARPES measurements [27].

ARPES measurements with UV photons were performed using SCIENTA SES-200 and SES-2002 spectrometers with a high-flux discharge lamp at Tohoku University, and at the undulator 4 m NIM beam line in the Synchrotron Radiation Center, Wisconsin. The energy and angular (momentum) resolution were set to 10–20 meV and 0.3° (0.01 $Å^{-1}$), respectively. X-ray ARPES measurements were performed with an SES-200 spectrometer at the undulator beamline BL25SU in SPring-8 with the energy and momentum resolutions of 200 meV and 0.03 $Å^{-1}$, respectively. Samples were cleaved *in situ* along the (0001) plane for MgB_2 and AlB_2, and the (001) plane for CaB_6 in an ultrahigh vacuum better than 2×10^{-10} Torr to obtain a clean surface. The Fermi level (E_F) of samples was referred to that of a gold film evaporated on the sample substrate.

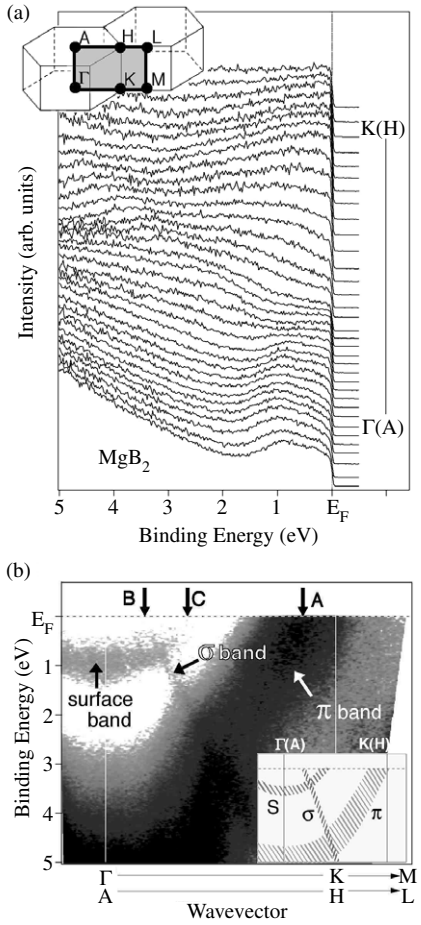

Figure 1. (a) ARPES spectra of MgB_2 measured at 45 K along the ΓKM(AHL) direction in the Brillouin zone (inset) with 28 eV photons. (b) ARPES-intensity plot of MgB_2 as a function of wavevector and binding energy. Arrows A, B, and C indicate the location of Fermi-level crossing points for the π, σ, and surface bands, respectively. The inset shows a schematic view of the band dispersion.

3. Results and discussion

3.1. Magnesium and aluminium diborides: MgB_2 and AlB_2

Figure 1(a) shows ARPES spectra of MgB_2 measured along the ΓKM (AHL) direction (see the inset) with 28 eV photons at 45 K. We find several band dispersions which cross E_F in this momentum region. To visualize the band dispersion more clearly, we plot the ARPES intensity as a function of wavevector and binding energy in figure 1(b), where dark areas correspond to the experimentally determined bands. We find three distinct band dispersions. The first one is a large electron-like band which crosses E_F near the K(H) point. The second one is a hole-like dispersion centred at Γ(A), crossing E_F near Γ(A). The third one is a small electron-like pocket centred at Γ(A). This result is consistent with the previous ARPES report by Uchiyama *et al* [28]. According to the band calculation [29], the first and second bands are attributed to the boron $2p_\pi$ and $2p_\sigma$ bands, respectively. The considerably broad feature of

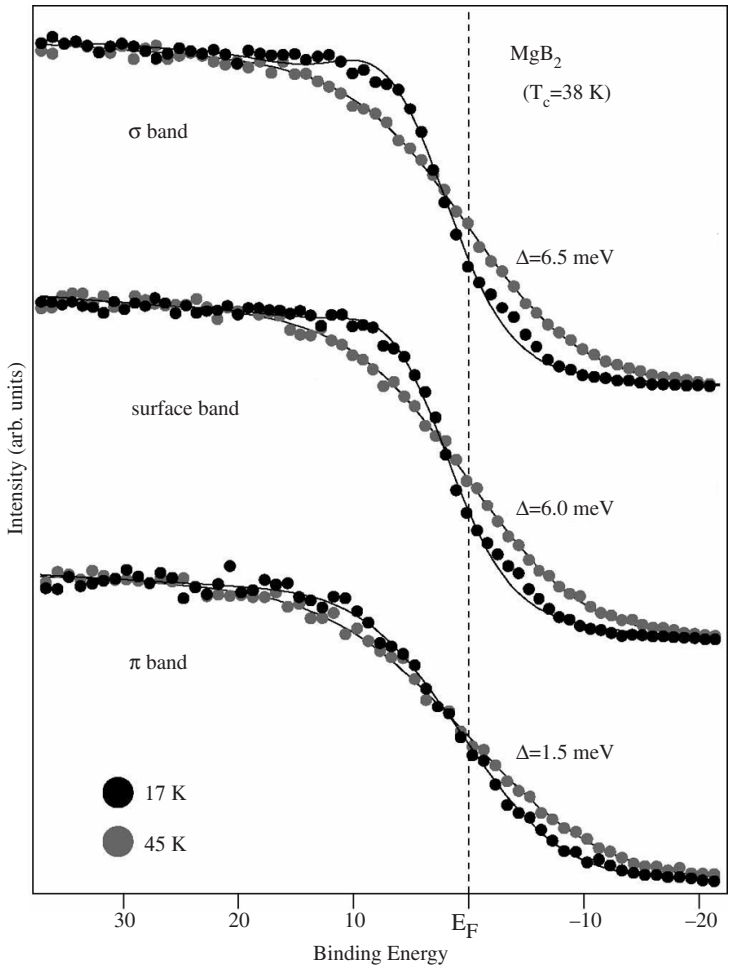

Figure 2. ARPES spectra near E_F of MgB_2 measured at two different temperatures (17 and 45 K) above and below T_c (38 K). Spectra are measured at three points A, B, and C in figure 1(b), which correspond to the π, σ, and surface bands, respectively.

the π band reflects the three-dimensional nature, while the sharp σ band shows the strong two-dimensional character. In contrast to these two bands, the third band is not predicted in the band calculation, so we assign it to a surface band. Further discussion on this band will be provided later with comparative ARPES study on the isostructural compound, AlB_2. The observed clear difference in the E_F-crossing point among the three bands enables us to perform precise ARPES measurements to observe the superconducting gap separately.

We measured ARPES spectra in the vicinity of E_F at three different points on the Fermi surface (points A, B, and C in figure 1(b)) at two temperatures below and above T_c (17 and 45 K). The results are shown in figure 2. The ARPES spectrum from the σ band shows a remarkable temperature dependence which cannot be explained by the simple temperature effect due to the Fermi–Dirac (FD) function. The midpoint of the leading edge in the spectrum at 17 K is not at E_F but is shifted by about 2 meV toward the higher binding energy, while that at 45 K is located at E_F. This clearly indicates that a superconducting gap opens at 17 K in the σ band. We observe a small piling-up effect of spectral weight around 7–15 meV in

the 17 K spectrum, indicative of emergence of a superconducting coherent peak below T_c, as observed in other superconductors [30]. It is surprising that a similar gap-opening behaviour is observed in the surface band as seen in figure 2. This point will be discussed later in more detail. In contrast to the σ and surface bands, the π band does not show a clear gap-opening behaviour. The shift of midpoint of the leading edge at 17 K is much less (0–1 meV) and no clear piling-up effect around 10 meV is seen, suggesting that no or a very small superconducting gap opens in the π band. This reveals a clear difference in the contribution to the superconductivity among three bands, supporting the multi-band superconductivity scenario in MgB_2 [3, 4].

To estimate the gap size (Δ), we numerically fitted the spectrum by the BCS spectral function with an integrated-type background representing the incoherent part of the spectral function and inelastically scattered electrons, multiplied by the FD function and convoluted with the energy resolution, as has been employed in high-T_c cuprates [31]. As shown in figure 2, ARPES spectra at 17 K for the σ, π, and surface bands are satisfactorily fitted with the gap size of $\Delta = 6.5 \pm 0.5$, 1.5 ± 0.5, and 6.0 ± 0.5 meV, respectively, with the broadening factor of 1.0 meV for the σ and surface bands and 0.5 meV for the π band. A slight deviation above E_F observed for the σ and surface bands may be due to a normal metallic region at the surface [32]. From the viewpoint of gap size, it is regarded that the present ARPES has observed 'two' gaps in MgB_2 since the size is almost the same between the σ and surface bands. So far many experiments, in particular tunnelling spectroscopy, have reported the multi-gap feature in MgB_2 and the reported gap sizes are roughly categorized into two groups, small and large superconducting gaps. The small gap has a value of 1–4 meV while the large one has 5.5–10 meV. The present ARPES result shown above seems to be consistent with these previous reports.

The two-gap nature in MgB_2 reported by previous studies has been interpreted by several models: (i) the simultaneous observation of the genuine bulk superconductivity and the weakened superconductivity in the surface layer [6, 7], (ii) the proximity effect in a thin metallic surface layer [8], (iii) the strongly anisotropic coupling to phonons [9], (iv) the contribution from the σ and π bands, which give the large and small gaps, respectively [3, 4], and (v) the same as (iv) but the correspondence between the band and the gap size is opposite, namely the π band produces a large gap [5]. It is clear from the present ARPES results that the σ and the surface bands have a large gap of 6–7 meV while the π band shows a small gap of 1–2 meV. Taking account of the fact that the superconductivity of MgB_2 is of bulk nature [1, 10], we conclude that the σ band plays a dominant role for the superconductivity of MgB_2 with a stronger coupling to phonons, while the π band is less important to the superconductivity with a much weaker coupling. This unambiguously indicates that the two-band model [3, 4] is the most appropriate to describe the superconductivity of MgB_2.

It is also inferred from the present ARPES results that the large gap observed by surface-sensitive techniques such as tunnelling spectroscopy may be due to both the σ and the surface bands, since the gap size is almost the same for the two bands. A large variation in the size of the large gap may stem from the various surface conditions depending on the surface preparation method. Although the reason why the surface band exhibits a similar gap size to the σ band is unclear at present, the proximity of the two bands in the momentum and energy spaces as seen in figure 1 may account for it, since the interaction between the surface and σ bands is expected to be larger than that between the surface and π bands.

Figures 3(a) and (b) show valence-band spectra of AlB_2 measured along the ΓKM(AHL) direction with the He IIα and He Iα resonance lines (40.814 and 21.218 eV), respectively. In figure 3(a), we find a prominent feature which is located at 5 eV at the Γ(A) point. This peak shows an upward dispersion from the Γ(A) point and approaches E_F near the K(H) point. We also find a broad hump structure near E_F, as indicated by triangles. This band looks to cross

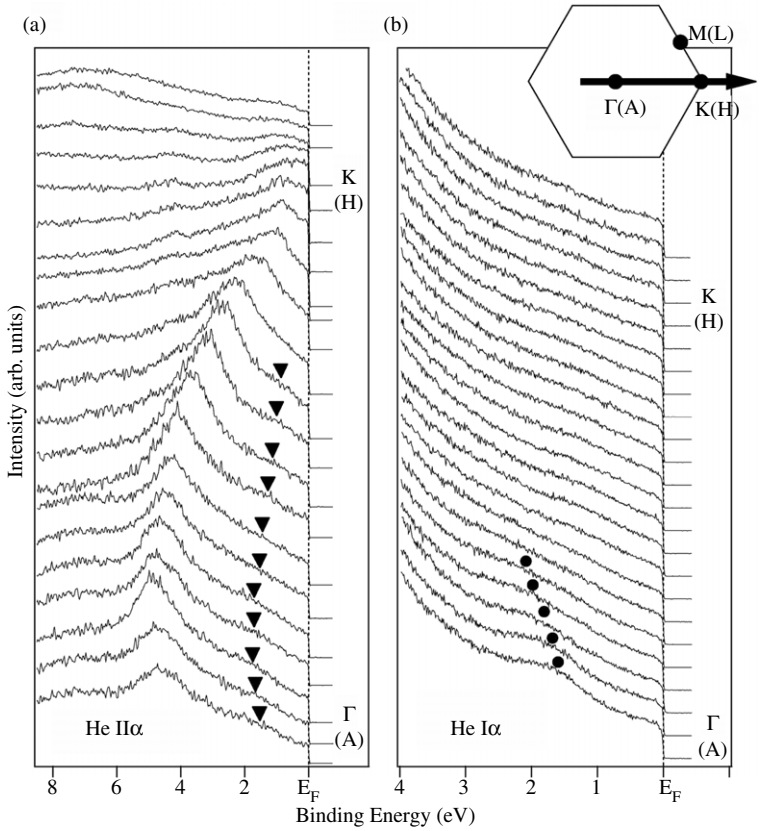

Figure 3. ARPES spectra of AlB_2 measured along the ΓKM(AHL) direction with He IIα (a) and He Iα (b) photons at 20 K. Filled circles and triangles are guides for the eyes to trace the band dispersion.

E_F around the midpoint between Γ(A) and K(H) points. In contrast to the highly dispersive feature of peaks in the He IIα spectrum, the He Iα spectrum (figure 3(b)) shows relatively weak angular dependence. However, we observe that a broad peak located at 1.5 eV at Γ(A) point shows a small dispersion as indicated by black circles.

In order to map out the band structure of AlB_2, we took the second derivative of the ARPES spectra in figure 3 after moderate smoothing and plotted the intensity as a function of wavevector and binding energy in figure 4(a). Since the observed dispersive feature is different between the He I and He II spectra (figures 3(a) and (b)), we added the intensity of both spectra and show the result in figure 4(a). The dark areas correspond to the experimentally determined bands. Figure 4(b) shows the calculated band structure of AlB_2 [33]. As seen in figure 4, it is obvious that bands u2 and u3 show a good agreement with the calculated σ (σ_1, σ_2) and π bands, respectively, while band u1 seems to correspond to the Al 3s band, but the energy position is substantially different. It is clear that the σ band in AlB_2 is totally occupied and therefore does not contribute to the Fermi surface. Band u3 shows a large electron-like dispersion centred at the Γ(A) point and crosses E_F near the K(H) point, forming a small hole pocket around the K(H) point. Band u1 shows an electron-like dispersion centred at the Γ(A) point and crosses E_F midway between the Γ(A) and K(H) points. Band u1 has the bottom at 1.6 eV, slightly overlapping with the top of band u2 at Γ(A) point, while the LDA calculation

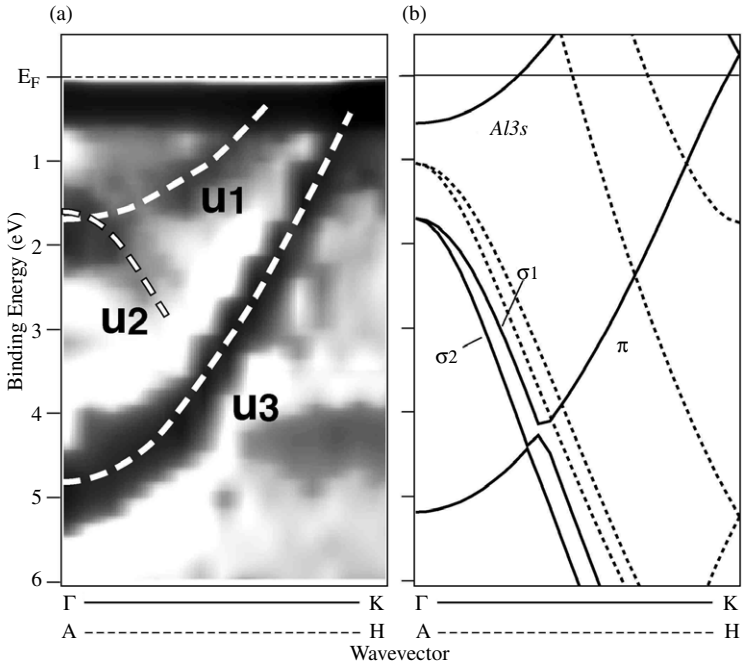

Figure 4. (a) Experimental band structure of AlB_2 determined by UV ARPES. Dark areas correspond to the bands. White broken lines are a guide for the eyes. (b) LDA band calculations for AlB_2 [33]. Solid and broken lines are calculated band dispersions along ΓK and AH high-symmetry lines, respectively.

predicts that the bottom of the Al 3s band is located close to E_F and is well separated from the σ bands by 1 eV at the Γ point. This discrepancy between band u1 and the calculated Al 3s band is significantly large, compared to the case of bands u2 and u3, whose energy positions correspond well to the calculated ones. It is noticed here that the discrepancy between the ARPES result and the LDA calculation for the electron pocket at the Γ(A) point is also seen in MgB_2. This suggests that the discrepancy observed in AlB_2 has the same origin as in MgB_2.

In order to elucidate the key factor for the superconductivity in MgB_2, we compare the ARPES results on AlB_2 with those on MgB_2. As in AlB_2, there are three bands seen near E_F in MgB_2, namely σ and π bands, and an additional parabolic band which forms an electron pocket at the Γ(A) point. The dispersive feature of these bands is similar between AlB_2 and MgB_2, but the energy position is different. The most striking difference occurs in the occupancy of the σ band. The σ band in AlB_2 is fully occupied with the top of the dispersion at 1.5 eV below E_F, in sharp contrast to the partially occupied σ band in MgB_2. On the other hand, the π band crosses E_F near the K(H) point in both compounds, indicating that both AlB_2 and MgB_2 have a π-band Fermi surface around the K(H) point. The electron pocket at the Γ(A) point also crosses E_F at the midpoint between Γ(A) and K(H) points in both compounds. This suggests that the partially occupied nature of the σ band, namely the hole-like Fermi surface originating in the σ band, is essential for the occurrence of superconductivity in MgB_2 in support of the two-band model [3, 4].

Next, we discuss the origin of the discrepancy in band u1. We think that there are two possibilities: (1) the LDA calculation overestimates the bandgap between the Al 3s and σ bands, and (2) band u1 is not the Al 3s band, but the surface band. To clarify this point, we

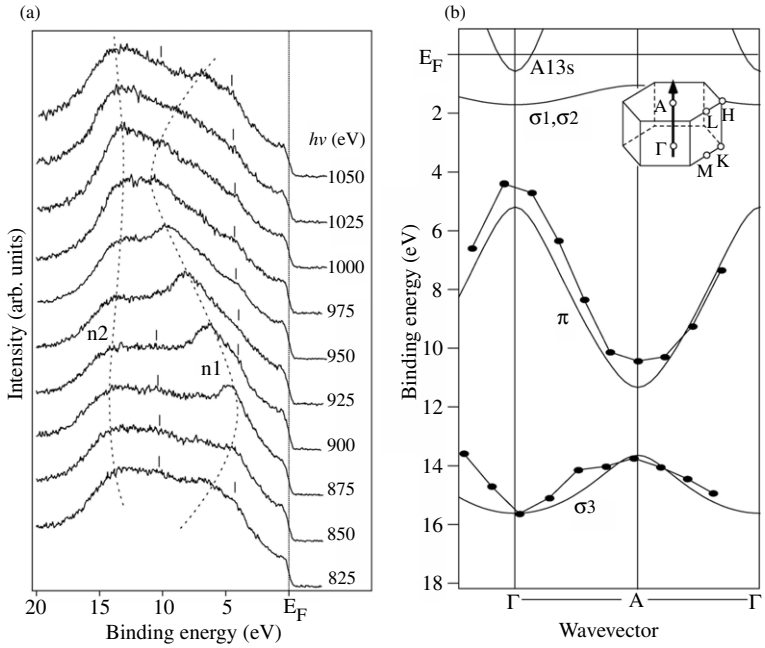

Figure 5. (a) Normal emission ARPES spectra of AlB_2 measured with x-rays of 825–1050 eV. Dashed lines are a guide for the eyes to trace the dispersion of bands n1 and n2. Bars show peak positions invariant with photon energy. (b) Plot of energy positions of dispersive bands n1 and n2 as a function of wavevector converted from photon energy with inner potential $V_0 = 15$ eV. Solid smooth lines are the LDA band calculations along the ΓA line [33].

performed x-ray ARPES, which is in general more bulk sensitive. Figure 5(a) shows normal emission ARPES spectra measured with 825–1050 eV photons, which trace the Γ–A line as shown in the inset of figure 5(b). We find two clear dispersive features n1 and n2 as indicated by dashed lines. Since both features show a band-back-folding at the same photon energies 875 and 975 eV, we attribute those to bulk electronic states, and the two photon energies correspond to the two different high symmetry points on the Γ–A line. We also find non-dispersive features at 5 and 10 eV as indicated with bars in figure 5(a). Since these energies correspond well to the top and bottom of the dispersive n1 band, we infer that these features come from angle-integrated type background due to elastic scattered photoelectrons. In figure 5(b), we plot the energy positions of peaks in the normal emission spectra as a function of wavevector on the Γ–A line by assuming a free-electron final state with an inner potential $V_0 = 15$ eV. In plotting the experimental data, we took account of finite momentum of photons, which is usually neglected in the case of UV photons. By comparing the experimental results with the band calculation, we attribute the two dispersive features n1 and n2 to the π and σ_3 bands, respectively. A relatively large bandwidth of the π band in the Γ–A direction reflects the three-dimensionality of the π band in contrast to the two-dimensional σ band confined within the honeycomb boron layer in the crystal.

Figure 6(a) shows the experimental band structure in the ΓKM(AHL) direction obtained by x-ray ARPES with 875 eV photons. In comparison with the result from UV ARPES (figure 4(a)), we find several agreements and disagreements. We find that band u3 in figure 4(a), which is assigned to the π band, shows a good agreement with band x1 in figure 6(a). We also find that band u2 in figure 4(a) corresponds to band x2 in figure 6(a), because both show a

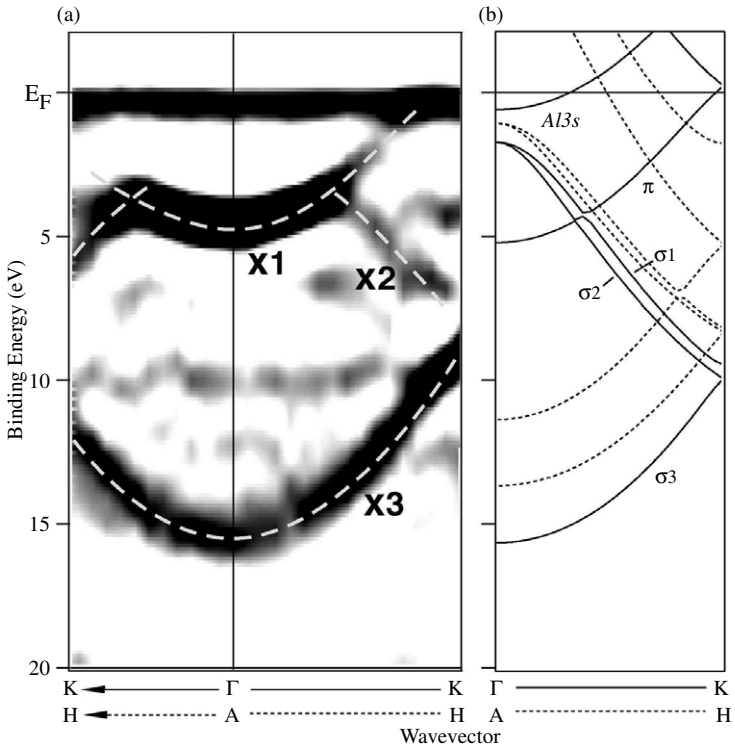

Figure 6. (a) Experimental band structure of AlB_2 determined by x-ray ARPES. Dark areas correspond to the bands. White broken lines are a guide for the eyes. (b) LDA band calculations along ΓK and AH lines [33].

similar upward dispersion toward the Γ(A) point. These bands (u2 and x2) are attributed to the σ (σ_1 and σ_2) band in the band calculation. In x-ray ARPES, this σ band is strongly suppressed around the Γ(A) point, possibly due to the k-dependent matrix element effect, as observed in the ARPES work on graphite [34]. In contrast to u2 and u3 bands, there is no counterpart of band u1 in the x-ray ARPES result. We have not observed any electron-pocket-like structure corresponding to band u1 in figure 4 for all the photon energies (825–1050 eV) which fully cover the momentum from Γ to A points as shown in figure 5. Considering the high surface sensitivity of UV photoemission, we conclude that band u1 in AlB_2 is a surface-originated band. For the reason described above, the electron pocket at the Γ(A) point in MgB_2 is also ascribed to a surface state. In fact, the band calculation on the MgB_2 surface predicts an electron pocket at the Γ point, supporting the present result [35, 36]. When we assign band u1 to the surface state, it means that the Al 3s band is not observed in ARPES. This suggests that the LDA calculation underestimates the gap between the Al 3s and σ bands. Or, Al vacancies in the crystal [37] may account for the absence of the Al 3s band below E_F, because Al vacancies cause the downward shift of the chemical potential (E_F) as observed in XAS/XES experiments on AlB_2 [38].

3.2. Calcium hexaboride: CaB_6

Figure 7(a) shows valence-band ARPES spectra of CaB_6 measured along the [100] (ΓX) direction with the He Iα resonance line (21.218 eV) at 30 K. Figure 7(b) shows the expansion

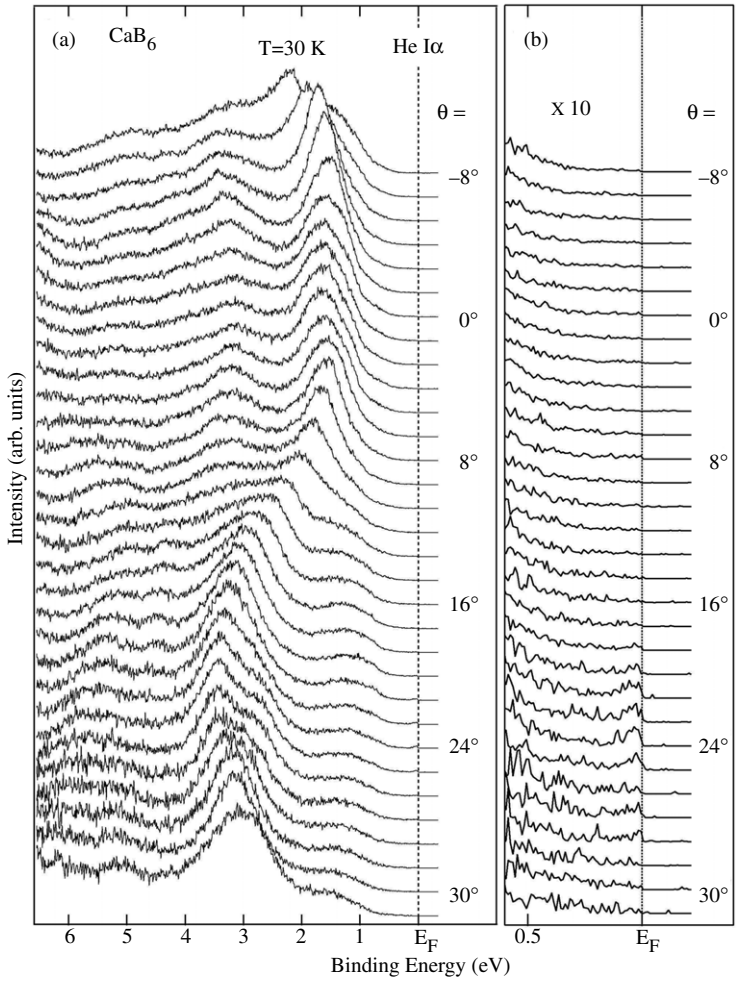

Figure 7. (a) Valence-band ARPES spectra of CaB_6 measured along the ΓX direction with He Iα photons (21.218 eV) at 30 K. The polar angle (θ) referred to the surface normal is indicated. (b) Expansion of the spectra near E_F.

of the same spectra near E_F. Prominent structures in the valence-band ARPES spectra, which show a systematic dispersion in the binding energy of 1–4 eV, are ascribed to the B 2p–2s hybridized states of the B_6 octahedron in the crystal. We also find additional small structures in the higher binding-energy region, also ascribable to the B 2p–2s states with a relatively higher B 2s weight. In contrast, no or negligible features are seen in the vicinity of E_F in the intensity scale of figure 7(a), although the expansion of spectra near E_F suggests a small structure around the X point. We discuss this small structure in detail later.

Figure 8(a) shows the ARPES-derived band structure of CaB_6, which is obtained by taking the second derivative of ARPES spectra in figure 7(a) after moderate smoothing and plotting the intensity as a function of the wavevector and the binding energy. The dark areas correspond to the experimental bands. The dispersion of experimental bands matches quite well with the periodicity of the bulk Brillouin zone, suggesting that the peaks/structures in the ARPES spectra originate in the bulk electronic structure, in particular, from the high-symmetry lines in the

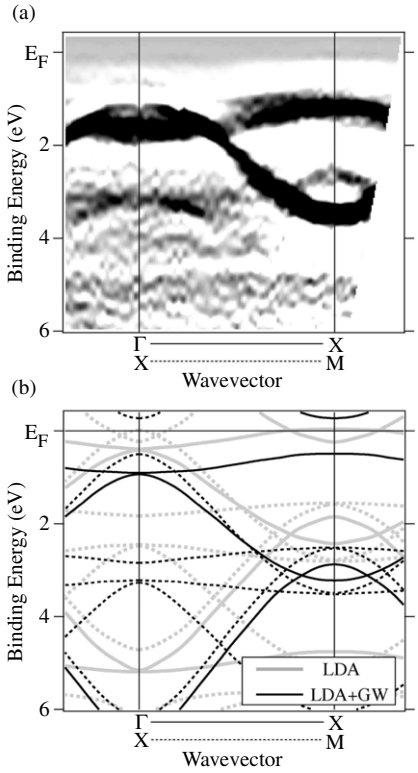

Figure 8. (a) Experimental band structure along ΓX of CaB_6 determined by ARPES. Dark areas correspond to bands. (b) LDA [40] and LDA + GW [41] band calculations of CaB_6.

bulk Brillouin zone, ΓX and XM. The experimental result in figure 8(a) is consistent with the previous ARPES study [39]. Figure 8(b) also shows a comparison of two different band calculations; LDA [40] and LDA + GW [41]. It is obvious that the LDA band calculation is shifted as a whole toward E_F with respect to the experiment, although the gross feature in the band dispersions looks similar. The fatal disagreement lies in the region near E_F at the X point, where the LDA calculation predicts a dispersive band which forms a hole pocket at the X point while the corresponding experimental band is situated far away (about 1 eV) from E_F at the X point. In contrast, the LDA + GW calculation shows a good agreement with the ARPES result; a highly dispersive band from Γ(X) to X(M) points shows an almost perfect agreement and a relatively flat band near E_F around the X point is qualitatively well reproduced in the LDA + GW calculation.

The next question is whether this energy gap is an intrinsic semiconducting gap as predicted from the LDA + GW calculation [41] or an energy gap created by formation of excitons (excitonic-insulator gap) as proposed by the excitonic-insulator model [20–23]. According to the theory [20–23], the energy of the excitonic-insulator gap is comparable to the transition temperature of ferromagnetism, 600 K (50 meV) [2, 42]. As shown in figure 8(a), however, the observed gap has an energy of 1 eV (12 000 K). This large difference in the energy scale indicates that the 1 eV energy gap at the X point is an intrinsic semiconducting energy gap, not due to the formation of excitons.

The surface sensitivity of UV ARPES raises a possibility that the semiconductive band structure may originate in the surface, but not the bulk. To examine this point, we have

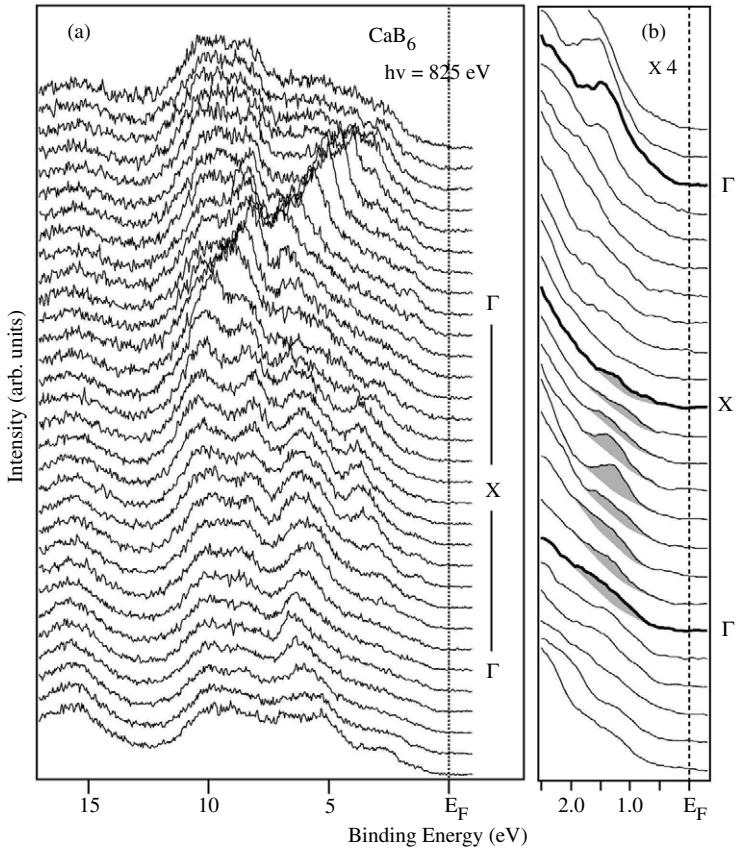

Figure 9. (a) X-ray ARPES spectra of $Ca_{0.995}La_{0.005}B_6$ measured along the ΓX direction with 825 eV photons at 20 K. (b) Spectra near E_F in the expanded intensity scale.

performed x-ray ARPES, which is more bulk sensitive than UV ARPES. Figure 9(a) shows the valence-band x-ray ARPES spectra of $Ca_{0.995}La_{0.005}B_6$ measured along the [100] (or ΓX) direction with 825 eV photons at 20 K. Figure 9(b) shows the enlargement in the near-E_F region. We find several bands in the binding-energy range of E_F–15 eV and they show a systematic and remarkable energy dispersion as a function of angle (namely momentum). Although the ARPES intensity is relatively weak near E_F, a small but distinct structure is seen at 1–1.5 eV between Γ and X points, as shown in figure 9(b).

Figure 10(a) shows the band structure of $Ca_{0.995}La_{0.005}B_6$ derived from the present x-ray ARPES. The experimental band structure is almost symmetric with respect to the high-symmetry points in the bulk Brillouin zone, indicating that the present x-ray ARPES certainly probes the bulk band structure. According to the band calculations, all bands in this energy range are ascribed to the B 2s–2p hybridized states of the B_6 octahedron in the crystal, with a stronger B 2s weight in the higher binding energy. In figure 10(a), we also show the LDA + GW band calculation [41] for comparison. The calculated bands are shifted as a whole toward the high binding energy by 0.3 eV. This shift corresponds to the chemical shift estimated on the assumption that 0.5% Ca atoms are replaced with the same number of La atoms in the calculated band structure. A good agreement in the energy position and the dispersion of bands is observed between the experimental band structure and the LDA + GW band calculation.

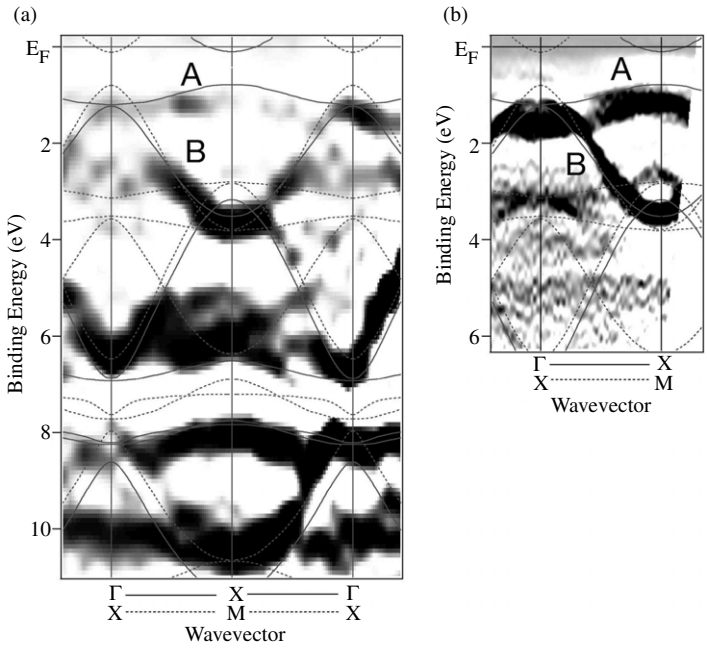

Figure 10. (a) Experimental band structure of $Ca_{0.995}La_{0.005}B_6$ determined by x-ray ARPES. Dark areas correspond to bands. The GW band calculation (solid and broken curves) [41] is superimposed for comparison. (b) Experimental band structure of CaB_6 determined by UV ARPES (the same as figure 8(a)).

Next we compare the x-ray ARPES results with those from the UV ARPES to study the possible surface effect on the electronic band structure in CaB_6. We show in figure 10(b) the band structure derived from figure 8(a) in the same energy and momentum scales as in figure 10(a). Because of the relatively small energy of ultraviolet light, the band structure only near E_F (E_F—4 eV) is observed in the experiment. In the band structure obtained by UV ARPES, there are two characteristic bands (bands A and B). Band A shows a relatively small energy dispersion with the top and the bottom of the band at X(M) and Γ(X) points, respectively. In contrast, band B has the top of the dispersion at the Γ(X) point, showing a remarkable downward dispersion toward the X(M) point. These two characteristic experimental bands are well reproduced in the LDA + GW band calculation [41], but not in the LDA calculations [40, 43, 44]. As shown in figure 10(a), these two characteristic bands are also observed in the experimental band structure obtained by x-ray ARPES, although the dispersive feature is not so clear as in the UV ARPES. It is remarked that the energy position of the two bands is almost the same between the x-ray and UV ARPES results, despite the large difference in the photon energy. We have performed similar x-ray ARPES measurements with several different energies of 800–900 eV and found no bands in the binding-energy range from E_F to 1 eV. By taking account of the fact that the present sample ($Ca_{0.995}La_{0.005}B_6$) is electron doped and the chemical potential should be situated at the bottom of the conduction band, the present finding by x-ray ARPES indicates that there is a 1 eV energy gap between the top of the valence band and the bottom of the conduction band in CaB_6, as suggested by UV ARPES. Since the energy gap of 1 eV is too large to be accounted for in terms of the formation of excitons whose binding energy should be comparable to the Curie temperature (600 K = 50 meV), the observed 1 eV gap is ascribed to the genuine semiconductor gap. The existence of a 1 eV gap

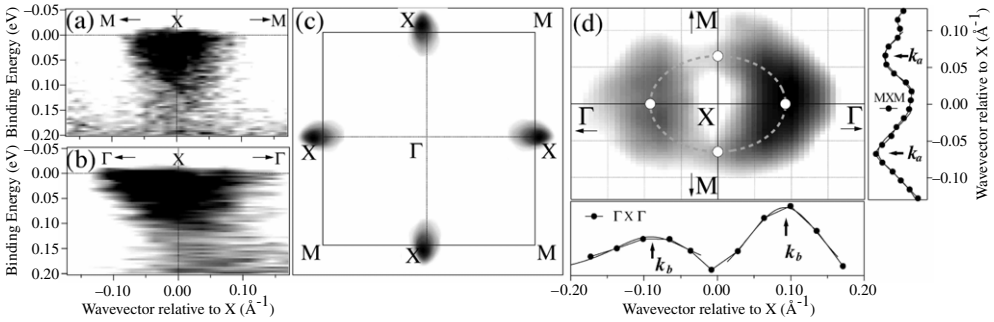

Figure 11. (a) and (b) ARPES-intensity plot near E_F around the X point along two directions, MXM and ΓMΓ. (c) Fermi surface of CaB_6 determined by plotting the ARPES intensity integrated over ±20 meV with respect to E_F. (d) Intensity map of $|\text{grad}_k n(\mathbf{k})|$ together with $|\text{grad}_k n(\mathbf{k})|$ cut along ΓMΓ (bottom panel) and MXM (right panel). The broken white line shows a locus of $\mathbf{k}_F$ positions determined by tracing the local maximum of $|\text{grad}_k n(\mathbf{k})|$.

at E_F in CaB_6 obviously contradicts the starting point of the excitonic insulator model, which assumes the semi-metallic band structure of CaB_6.

Although the semiconductive band structure of CaB_6 is definitive as described above, the observed large semiconducting gap seems to apparently contradict the metallic nature of the sample. This discrepancy may be resolved by the small structure near E_F around the X point as shown in figure 7(b). In order to study the detailed electronic structure near E_F, we have measured ARPES spectra along many cuts in the Brillouin zone and found that this small structure is localized only around the X point. Figures 11(a) and (b) plot the ARPES intensity near E_F around the X point in the two directions, XM and XΓ, respectively, where we clearly find a small dispersive feature, indicating a small electron-like Fermi surface centred at the X point. The ARPES intensity is distributed more widely in the XΓ direction than in the XM direction, indicative of a spheroidal shape of the Fermi surface. This is more clearly seen in figure 11(c), where the ARPES intensity near E_F (±20 meV with respect to E_F) is plotted in the two dimensional Brillouin zone. Figure 11(c) clearly shows that the CaB_6 single crystal used in the present ARPES measurement has a small electron-like spheroidal Fermi surface elongated along the XΓ direction centred at the X point. This means that the CaB_6 crystal is already doped, probably due to defects or deficiencies in the crystal. This small Fermi surface gives the metallic nature to the sample, consistent with the electrical resistivity of the sample.

Next we estimate the volume of the Fermi surface, namely the carrier number, from the ARPES experiment. Figure 11(d) shows the intensity of $|\text{grad}_k n(\mathbf{k})|$, where $n(\mathbf{k})$ is the momentum distribution function defined with the ARPES spectral intensity near E_F integrated from 50 meV above E_F to 150 meV below E_F. We have estimated the Fermi vectors measured from the X point in the XM and XΓ directions ($\mathbf{k}_a$ and $\mathbf{k}_b$) by taking the maximum point of $|\text{grad}_k n(\mathbf{k})|$ [45] as shown in figure 11(d). They are 6.5×10^{-2} and 9.2×10^{-2} Å^{-1} for the shorter $\mathbf{k}_a$ and longer $\mathbf{k}_b$ axes, respectively. By assuming a perfect spheroidal shape, we have estimated the volume of the Fermi surface to be 2.8×10^{-3} of the whole Brillouin-zone volume, which corresponds to the carrier number of 3.9×10^{19} cm^{-3}. In order to independently estimate the character and the number of carriers, we also performed Hall resistivity measurements with the same CaB_6 crystal as used in the ARPES measurement. The Hall resistivity measurement shows that the sign of the carrier is negative and the number of carriers at 30 K is 5.2×10^{19} cm^{-3}, which shows an excellent agreement with the ARPES result. All these indicate that the CaB_6 single crystal used in the present study has a small electron-like

spheroidal Fermi surface centred at the X point in the Brillouin zone and the volume (carrier number) is 4–5 $\times$ 10^{19} cm^{-3}.

Finally, we discuss possible mechanisms for the novel ferromagnetism in doped CaB_6 based on the present ARPES results. The band structure determined by ARPES (figures 8 and 10) clearly shows that a large (1 eV) intrinsic gap opens between the conduction and the valence bands at the X point in the Brillouin zone. This is in sharp contrast to the essential starting point of the excitonic-insulator model [20–23], which assumes overlapping of an electron and a hole pocket at E_F. The 1 eV energy gap is hardly accounted for in terms of the formation of excitons. In contrast, the present ARPES results seem to favour the low-density electron–gas model [24, 25]. In fact, the obtained carrier density (4–5 $\times$ 10^{19} cm^{-3}) lies in the predicted polarized-fluid region (10^{18}–10^{20} cm^{-3}) between the Fermi-liquid and the Wigner-crystal region [24, 25]. A remaining problem is how the electrons in the small Fermi surface with a strongly anisotropic t_u molecular-orbital nature give rise to the high-temperature ferromagnetism as free electrons in the low-density electron–gas model where no anisotropic wavefunction is supposed [24, 25].

Next we discuss the possibility of the surface ferromagnetism based on the present ARPES results. It has been theoretically suggested that the weak ferromagnetism of CaB_6 is due to the magnetized B_6 vacancies produced on the [001] cleaved surface [46]. These B_6 vacancies are expected to accumulate the negative charge on the surface and would produce a small electron pocket at the Fermi level through the chemical potential shift. The small electron pocket at the X point observed by UV ARPES is not found in x-ray ARPES, suggesting the surface nature of the electron pocket. However, it is remarked that the energy position of each band (bands A and B) in figure 10 derived from UV ARPES agrees well with that determined by bulk sensitive x-ray ARPES. This clearly indicates that there is no band-bending at the surface due to the charged B_6 vacancies, eliminating the possible surface magnetism. In return, the good agreement in the energy position of bands between UV and x-ray ARPES suggests that the small electron pocket at the X point is of bulk origin. Since the ARPES signal from this electron pocket is very small even in UV ARPES [27, 39], no clear observation of this structure in x-ray ARPES may be due to the insufficient energy resolution and/or the low photoionization cross-section. Considering that a ferromagnetic sample always shows metallic conductivity, the electron pocket at the X point may be related to the reported weak ferromagnetism.

4. Conclusion

We have performed UV and x-ray ARPES on two novel borides, MgB_2 and CaB_6, to study the electronic structure and the Fermi surface relevant to the interesting and anomalous properties observed in these compounds. In MgB_2, we have succeeded in observing the superconducting gaps of the σ and π bands separately. We found that the superconducting gap of the σ band (6.5 $\pm$ 0.5 meV) is remarkably larger than that of the π band (1.5 $\pm$ 0.5 meV). We also found that the σ band is totally occupied in AlB_2, which is a non-superconducting isostructural reference of MgB_2. These indicate that the partially filled σ band is essential for the two-band superconductivity in MgB_2. In addition to the σ and π bands, we observed a small electron-like pocket at the Γ point, which we ascribe to the surface states by comparative UV and x-ray ARPES measurements. In CaB_6, we found that an energy gap of 1 eV opens at the X point between the valence and conduction bands. The absence of overlapping of electron and hole Fermi surfaces in CaB_6 suggests that the ferromagnetism observed in doped CaB_6 is not accounted for by the formation of excitons. Instead, we observed a small spheroidal electron-like Fermi surface at the X point in doped CaB_6. The estimated carrier number lies in the region where a weak ferromagnetism is predicted in the low-density electron–gas model.

Acknowledgments

This work was done in collaboration with T Sato, H Matsui, H Komatsu, A Kaminski, J C Campuzano, S-C Wang, H Ding, Y Machida, S Sasaki, K Kadowaki, Y Umeda, N Kimura, H Aoki, S Kunii, R Kaji, T Sasaki, Y Yokoo, and J Akimitsu. We also thank H Kumigashira, T Ito, T Matsumura, Y Iida, T Muro, and H Hochst for their collaboration in measurements. This work was supported by a grant from the MEXT of Japan.

References

[1] Nagamatsu J, Nakagawa N, Muranaka T, Zenitani Y and Akimitsu J 2001 *Nature* **410** 63–4
[2] Young D P, Hall D, Torelli M E, Fisk Z, Sarrao J L, Thompson J D, Ott H R, Oseroff S B, Goodrich R G and Zysler R 1999 *Nature* **397** 412–4
[3] Liu A Y, Mazin I I and Kortus J 2001 *Phys. Rev. Lett.* **87** 087005
[4] Choi H J, Roundy D, Sun H, Cohen M L and Louie S G 2002 *Nature* **418** 758–60
[5] Joas C, Eremin I, Manske D and Bennemann K H 2002 *Phys. Rev.* B **65** 132518-1-4
[6] Karapetrov G, Iavarone M, Kwok W K, Crabtree G W and Hinks D G 2001 *Phys. Rev. Lett.* **86** 4374–7
[7] Schmidt H, Zasadzinski J F, Gray K E and Hinks D G 2001 *Phys. Rev.* B **63** 220504(R)
[8] McMillan W L 1968 *Phys. Rev.* **175** 537–42
[9] Seneor P, Chen C T, Yeh N C, Vasquez R P, Bell L D, Jung C U, Park M S, Kim H J, Kang W N and Lee S I 2002 *Phys. Rev.* B **65** 012505
[10] Bouquet F, Fisher R A, Phillips N E, Hinks D G and Jorgensen J D 2001 *Phys. Rev. Lett.* **87** 047001
[11] Bouquet F, Wang Y, Sheikin I, Plackowski T, Junod A, Lee S and Tajima S 2002 *Phys. Rev. Lett.* **89** 257001
[12] Chen X K, Konstantinovic M J, Irwin J C, Lawrie D D and Franck J P 2001 *Phys. Rev. Lett.* **87** 157002
[13] Quilty J W, Lee S, Yamamoto A and Tajima S 2002 *Phys. Rev. Lett.* **88** 087001
[14] Szabo P, Samuely P, Kacmarcik J, Klein T, Marcus J, Fruchart D, Miraglia S, Marcenat C and Jansen A G M 2001 *Phys. Rev. Lett.* **87** 137005
[15] Gonnelli R S, Daghero D, Ummarino G A, Stepanov V A, Jun J, Kazakov S M and Karpinski J 2002 *Phys. Rev. Lett.* **89** 247004
[16] Giubileo F, Roditchev D, Sacks W, Lamy R, Thanh D X, Klein J, Miraglia S, Fruchart D, Marcus J and Monod P 2001 *Phys. Rev. Lett.* **87** 177008
[17] Schmidt H, Zasadzinski J F, Gray K E and Hinks D G 2002 *Phys. Rev. Lett.* **88** 127002
[18] Eskildsen M R, Kugler M, Tanaka S, Jun J, Kazakov S M, Karpinski J and Fischer O 2002 *Phys. Rev. Lett.* **89** 187003
[19] Tsuda S, Yokoya T, Kiss T, Takano Y, Togano K, Kito H, Ihara H and Shin S 2001 *Phys. Rev. Lett.* **87** 177006
[20] Zhitomirsky M E, Rice T M and Anisimov V I 1999 *Nature* **402** 251–3
[21] Balents L and Varma C M 2000 *Phys. Rev. Lett.* **84** 1264–7
[22] Barzykin V and Gor'kov L P 2000 *Phys. Rev. Lett.* **84** 2207–10
[23] Murakami S, Shindou R, Nagaosa N and Mishchenko A S 2002 *Phys. Rev. Lett.* **88** 126404
[24] Ceperley D 1999 *Nature* **397** 386–7
[25] Oritz G, Harris M and Ballone P 1999 *Phys. Rev. Lett.* **82** 5317–21
[26] Machida Y, Sasaki S, Fujii H, Furuyama M, Kakeya I and Kadowaki K 2003 *Phys. Rev.* B **67** 094507
[27] Souma S, Komatsu H, Takahashi T, Kaji R, Sasaki T, Yokoo Y and Akimitsu J 2003 *Phys. Rev. Lett.* **90** 027202
[28] Uchiyama H, Shen K M, Lee S, Damascelli A, Lu D H, Feng D L, Shen Z X and Tajima S 2002 *Phys. Rev. Lett.* **88** 157002
[29] Kortus J, Mazin II, Belashchenko K D, Antropov V P and Boyer L L 2001 *Phys. Rev. Lett.* **86** 4656–9
[30] Fedorov A V, Valla T, Johnson P D, Li Q, Gu G D and Koshizuka N 1999 *Phys. Rev. Lett.* **82** 2179–82
[31] Ding H, Campuzano J C, Bellman A F, Yokoya T, Norman M R, Randeria M, Takahashi T, Katayama-Yoshida H, Mochiku T, Kadowaki K and Jennings G 1995 *Phys. Rev. Lett.* **74** 2784–7
[32] Reinert F, Nicolay G, Eltner B, Ehm D, Schmidt S, Hufner S, Probst U and Bucher E 2001 *Phys. Rev. Lett.* **87** 047001
[33] Antropov V P, Belashchenko K D, Schifgaarde M v and Rashkee S N 2001 *Stud. High Temp. Supercond.* **38** 179
[34] Shirley E L, Terminello L J, Santoni A and Himpsel F J 1995 *Phys. Rev.* B **51** 13614–22
[35] Servedio V D P, Drechsler S-L and Mishonov T 2002 *Phys. Rev.* B **66** 140502(R)
[36] Silkin V M, Chulkov E V and Echenique P M 2001 *Phys. Rev.* B **64** 172512
[37] Loa I, Kunc K, Syassen K and Bouvier P 2002 *Phys. Rev.* B **66** 134101

[38] Nakamura J, Watanabe M, Oguchi T, Nasubida S Y, Kabasawa E, Yamada N, Kuroki K, Yamazaki H, Shin S, Umeda Y, Minakawa S, Kimura N and Aoki H 2002 *J. Phys. Soc. Japan* **71** 408–10
[39] Denlinger J D, Clack J A, Allen J W, Gweon G H, Poirier D M, Olson C G, Sarrao J L, Bianchi A D and Fisk Z 2002 *Phys. Rev. Lett.* **89** 157601
[40] Massidda S, Continenza A, dePascale T M and Monnier R 1997 *Z. Phys.* B **102** 83–9
[41] Tromp H J, van Gelderen P, Kelly P J, Brocks G and Bobbert P A 2001 *Phys. Rev. Lett.* **87** 016401
[42] Ott H R, Gavilano J L, Ambrosini B, Vonlanthen P, Felder E, Degiorgi L, Young D P, Fisk Z and Zysler R 2000 *Physica* B **281/282** 423–7
[43] Hasegawa A and Yanase A 1979 *J. Phys. C: Solid State Phys.* **12** 5431–40
[44] Rodriguez C O, Weht R and Pickett W E 2000 *Phys. Rev. Lett.* **84** 3903–6
[45] Straub T, Claessen R, Steiner P, Hufner S, Eyert V, Friemelt K and Bucher E 1997 *Phys. Rev.* B **55** 13473–8
[46] Monnier R and Delley B 2001 *Phys. Rev. Lett.* **87** 157204